RESEARCH ARTICLE

Robo1 promotes angiogenesis in hepatocellular carcinoma through the Rho family of guanosine triphosphatases' signaling pathway

Jian-Yang Ao [1,2,4] · Zong-Tao Chai [1,2,5] ·
Yuan-Yuan Zhang [1,2] · Xiao-Dong Zhu [1,2] ·
Ling-Qun Kong [3] · Ning Zhang [1,2] · Bo-Gen Ye [1,2] ·
Hao Cai [1,2] · Dong-mei Gao [1,2] · Hui-Chuan Sun [1,2]

Abstract Robo1 is a member of the Robo immunoglobulin superfamily of proteins, and it plays an important role in angiogenesis and cancer. In this study, we investigate the role of roundabout 1 (Robo1) in tumor angiogenesis in hepatocellular carcinoma (HCC). Firstly, the relationship between Robo1 expression on tumors and patient's survival and endothelial cells in tumor blood vessels and patient's survival was studied. Secondly, Robo1 was overexpressed or knocked down in human umbilical vein endothelial cells (HUVECs). Cell proliferation, motility, and tube formation were compared in HUVEC with different Robo1 expression. Also, HUVECs with different Robo1 expression were mixed with HCCLM3 and HepG2 hepatoma cells and then implanted in a nude mouse model to examine the effects of Robo1 in endothelial cells on tumor growth and angiogenesis. Cell motility-related molecules were studied to investigate the potential mechanism how Robo1 promoted tumor angiogenesis in HCC. The disease-free survival of the patients with high Robo1 expression in tumoral endothelial cells was significantly shorter than that of those with low expression ($P=0.021$). Overexpression of Robo1 in HUVECs resulted in increased proliferation, motility, and tube formation in vitro. In the implanted mixture of tumor cells and HUVECs with an increased Robo1 expression, tumor growth and microvessel density were enhanced compared with controls. Robo1 promoted cell division cycle 42 (Cdc42) expression in HUVECs, and a distorted actin cytoskeleton in HUVECs was observed when Robo1 expression was suppressed. In conclusion, Robo1 promoted angiogenesis in HCC mediated by Cdc42.

Jian-Yang Ao and Zong-Tao Chai contributed equally to this work.

Keywords Hepatocellular carcinoma · Angiogenesis · Roundabout receptors 1 · Rho GTPase

✉ Hui-Chuan Sun
sun.huichuan@zs-hospital.sh.cn

1   Liver Cancer Institute and Zhongshan Hospital, Fudan University, 180 Fenglin Road, Shanghai 200032, China

2   Key Laboratory of Carcinogenesis and Cancer Invasion, Ministry of Education, Shanghai 200032, China

3   Department of Hepatobiliary Surgery, Binzhou Medical College Affiliated Hospital, Binzhou, Shandong 256610, China

4   The First Affiliated Hospital of Wenzhou Medical University, Wenzhou 325000, China

5   Changhai Hospital, Second Military Medical University, Shanghai 200433, China

Abbreviations

HCC	Hepatocellular carcinoma
HUVEC	Human umbilical vein endothelial cell
GTPase	Guanosine triphosphatase
AFP	α-Fetoprotein
TEC	Tumor endothelial cell
Rho	Ras homolog family member
GAPDH	Glyceraldehyde-3-phosphate dehydrogenase

Introduction

Hepatocellular carcinoma (HCC) is the second leading cause of cancer death in men and the sixth leading cause of cancer death in women worldwide [1]. Most patients with HCC experience a recurrence after resection/ablation or are diagnosed at advanced stages. Active angiogenesis plays an important role in progression and metastasis of HCC [2–4], but the mechanisms responsible for HCC progression and metastasis are still not fully understood.

Sorafenib, an anti-angiogenesis therapy, has become the standard of care for patients with advanced HCC, but its efficacy is not satisfactory [5]. Although many other anti-angiogenesis drugs have been tested in phase III trials in first-line (brivanib, sunitinib, erlotinib, and linifanib) and/or second-line (brivanib and everolimus) settings, none of them showed superior effects compared with sorafenib [5]. Thus, more research on the mechanism of angiogenesis in HCC needs to be done.

Nerves and blood vessels use common genetic pathways [6, 7]. Roundabout receptors (Robo) play an important role in axon guidance and neuronal migration [8, 9], and they have been implicated in angiogenesis and cancer [10, 11]. Robo1 is a member of the Robo immunoglobulin superfamily of proteins [10]. Previous studies showed that Robo1 is a tumor suppressor in breast, prostate, gastric, and colorectal cancers [12–14], and it also functions as an oncogene in skin, nasopharyngeal, and gallbladder cancers [15–17]. In a melanoma xenograft model, neutralization of Robo1 on endothelial cells reduced tumor angiogenesis and tumor growth [11]. Expression of Robo1 was found on HCC cells, and monoclonal antibody against Robo1 on tumor cells exhibited antitumor activity in a HCC xenograft model [18]. However, it is still not clear whether Robo1 is expressed by endothelial cells in tumor vessels in HCC.

In this study, we investigated whether Robo1 expression promoted angiogenesis in HCC and explored its clinical significance and downstream pathway.

Materials and methods

Patients and specimens

Archived surgical specimens from 292 consecutive patients who underwent liver resection for HCC in our institute (Liver Cancer Institute, Fudan University) from March 2004 to December 2006 were collected as cohort 1. Fresh HCC and liver specimens from 81 patients who received liver resection for HCC in the same institute from January 2012 to November 2013 were collected as cohort 2. Hepatitis B history was defined as ever detectable serum hepatitis B surface antigen. Microvascular invasion was defined as the presence of tumor

cells within a vascular lumen lined by endothelium under microscopy [19]. The study was approved by the Zhongshan Hospital Research Ethics Committee. Informed consent was obtained from patients according to the hospital regulations.

Clinicopathological features of cohort 1 and 2 patients are detailed in Supplementary Tables 1 and 2. All the patients were histologically diagnosed as HCC. None of these patients received any preoperative anticancer treatment, including chemotherapy or anti-angiogenesis drugs. Patients were followed up every 2 months in the first postoperative year and at least every 3 months afterward. The median follow-up time of cohorts 1 and 2 were 32.4 and 9 months, respectively. Follow-up procedures were described in our previous report [20].

Cell lines

Human HCC cell lines HepG2 (Shanghai Institute of Cell Biology, Shanghai, China) and HCCLM3 (Liver Cancer Institute, Fudan University, Shanghai, China) were cultured in Dulbecco's modified Eagle's medium (Invitrogen, Carlsbad, CA, USA) containing 10 % fetal bovine serum in a humidified incubator at 37 °C with an atmosphere of 5 % CO_2. A human umbilical vein endothelial cell (HUVEC) line was purchased from AllCells (Shanghai, China). HUVECs were grown in an AllCells-completed medium supplemented with 10 % (v/v) fetal bovine serum at 37 °C in a humidified atmosphere with 5 % CO_2. Tumor endothelial cells (TECs) were obtained from fresh HCC specimens right after removal from patients with a positive α-fetoprotein (AFP; >20 ng/ml), as described previously [21], TECs were grown in an AllCells-completed medium supplemented with 10 % (v/v) fetal bovine serum at 37 °C in a humidified atmosphere with 5 % CO_2.

Immunohistochemical analysis

Paraffin-embedded tumor tissues were cut into 6-μm sections, and CD31 antibody staining (1:100; Abcam) or Robo1 antibody staining (1:100; Abcam) was performed on these sections. Frozen sections (5-μm) of tumor samples were used to determine the expression of Robo1 and CD31 using an anti-Robo1 antibody (1:100; Abcam) and an anti-CD31 antibody (1:100; Santa Cruz Biotechnology, TX, USA) by immunofluorescent staining. The positive staining area/integrated optical density (IOD) value was determined as described previously [20].

HUVECs and TECs growing on glass coverslips were fixed in 4 % paraformaldehyde for 15 min. The cells were then rinsed three times with phosphate-buffered saline (PBS) for 5 min each time and incubated in a protein-blocking solution for 30 min at room temperature. After incubation with the primary antibody against Robo1 or CD31 overnight at 4 °C, followed by incubation with the secondary antibody (Alexa Fluor 488 donkey anti-mouse, Alexa Fluor 546 donkey anti-

rabbit, 1:300; Jackson ImmunoResearch Laboratories Inc., PA, USA) at 37 °C for 2 h, the cells were counterstained with 4′,6-diamidino-2-phenylindole (DAPI) (Beyotime Biotechnology, Shanghai, China). Cells or slides not incubated with primary antibodies served as negative controls. The cells or slides were then analyzed by confocal laser scanning microscopy.

Cells were transfected with Robo1 (HUVEC-oe-Robo1), small interfering RNA (siRNA)-targeting Robo1 (HUVEC-kd-Robo1), or scramble oligomers (HUVEC-nc-Robo1). HUVEC-oe-Robo1, HUVEC-nc-Robo1, and HUVEC-kd-Robo1 cells growing on glass coverslips were fixed in 4 % paraformaldehyde for 15 min. The cells were then rinsed three times with PBS for 5 min and then incubated in a protein-blocking solution for 30 min at room temperature. After incubation with the primary FITC-phalloidin antibody (1:100, Yeasen, Shanghai, China) overnight at 4 °C, the cells were counterstained with DAPI (Beyotime Biotechnology, Shanghai, China) to reveal the nuclei. Cells or slides not incubated with primary antibodies served as negative controls. The cells or slides were then analyzed by confocal laser scanning microscopy.

The positive staining area of CD31 and Robo1 on vessels was measured with a computerized image system or via microscopy. Briefly, under ×400 magnification, four photographs of the representative fields were captured by a laser confocal (TCS SP8; Leica, Wetzlar, Germany) image system and analyzed with Image-Pro Plus version 6.2 software (Media Cybernetics Inc., Bethesda, MD, USA) [22]. A uniform setting for all the slides was applied to decrease the operational error. All positive staining of CD31 in each photograph was measured as vascular area, and only CD31 and Robo1 double-positive area was considered to be Robo1 staining on endothelial cells. The intensity of Robo1 expression on endothelial cells is presented as a ratio of Robo1 expression to CD31 expression. The IOD value of tumor cells is defined as Robo1 expression in tumors. Those patients with the ratio higher than the median value were defined as having high expression of Robo1 on endothelial cells/tumor cells.

We used nondestructive procedures of confocal laser scanning microscopy in combination with computer-assisted methods to visualize tumor vessels. Two independent sets of DAPI and mCherry images were collected and then merged into one image to give a three-dimensional impression at high light microscopic resolution and sensitivity [23].

Interfering with the expression of Robo1 and Cdc42 in endothelial cells

Synthetic siRNA oligonucleotides specific for regions in the Robo1 and Cdc42 messenger RNAs (mRNAs) were designed and synthesized by Sigma-Aldrich (St. Louis, MO, USA). The silencing effects of several siRNA oligonucleotides were screened and tested initially for their ability to silence Robo1 expression. The most effective oligonucleotides for Robo1 (5′-CACAAUGACUGCUCCAUCA-3′, sense) almost completely blocked its expression. The most effective oligonucleotides for Cdc42 (5′-AGAUUACGACCGCUGAGUU-3′, sense) almost completely blocked its expression. HUVECs in 60-mm dishes at 30–50 % confluency were transfected with siRNA oligonucleotides using Lipofectamine RNAiMAX (Invitrogen) for 24 h, and then the medium was changed with the fresh AllCells-completed medium. After 48 h, the cellular protein was collected. The control transfection was performed with Stealth RNAi Negative Control Duplexes (Sigma-Aldrich).

The human Robo1 gene was synthesized and inserted in the lentivirus (GeneChem, Shanghai, China) to obtain a Robo1 expression vector. We then generated the vector with the greatest capacity to reduce Robo1 expression and the negative control vector in HEK293 cells. These vectors, with their packaging vectors, were transfected into 293-T cells using Lipofectamine 2000 (Invitrogen). HUVECs were then transfected with virus following the manufacturer's instructions, and Western blot was used to measure Robo1 expression for validation. The vector-reducing Robo1 expression was U6-MCS-ubiquitin-Cherry-IRES-puromycin, and that upregulating Robo1 expression was Ubi-MCS-3FLAG-SV40-Cherry-IRES-puromycin.

Reverse transcription polymerase chain reaction analysis

Cells were transfected with vectors of Robo1 (HUVEC-oe-Robo1), siRNA-targeting Robo1 (HUVEC-kd-Robo1), or scramble oligomers (HUVEC-control). Total RNA from HUVECs described above was extracted and reverse transcribed into single-stranded complementary DNA (cDNA) using the iScript cDNA synthesis kit (Bio-Rad Laboratories, USA) following the manufacturer's instructions. For quantitative PCR, primers were designed by Sangon Biotech, Shanghai, China, and their efficiency was tested on a genomic DNA dilution series. Quantitative PCR was performed with the Applied Biosystems 8100 HT Sequence Detection System (Applied Biosystems, USA). Expression of the glyceraldehyde-3-phosphate gene was used to normalize the expression of each gene. The following primer sequences were used to determine the expression of the target gene: TGF-β [5′-CCTGCCTGTC TGCACTATTCC-3′ (forward); 5′-CCAAGGTGCTCAAT AAATAGATCTAACTAC-3′ (reverse)], proliferating cell nuclear antigen (PCNA) [5′-CCACTCCACTCTCTTCAACG G-3′ (forward); 5′-TACTCTACAACCAAGGGGTACAT CTG-3′ (reverse)], Cdc42 [5′-AAGAAAAGTGGGTGCC TGAGATAA-3′ (forward); 5′-GTCTCTGGAGTGATAGGC TTCTGTT-3′ (reverse)], EGFR [5′-GCGGCAGGACCAAG

CA-3′ (forward); 5′-CGTAATCCCAAGGATGTTATGT TCA-3′ (reverse)], cyclin-D1 [5′-CTGGGTCTGTGCATTT CTGGTT-3′ (forward); 5′-GCTGGAAACATGCCGGTTA-3′ (reverse)], and glyceraldehyde-3-phosphate dehydrogenase (GAPDH) [5′-CGGAGTCAACGGATTTGGTCGTAT-3′ (forward); 5′-AGCCTTCTCCATGGTGGTGAAGAC-3′ (reverse)].

Western blot analysis

The HUVEC-kd-Robo1 cells, HUVEC-oe-Robo1 cells, and their controls were lysed with RIPA Lysis Buffer (Santa Cruz Biotechnology, TX, USA) containing protease inhibitors (Beyotime Biotechnology, Shanghai, China). The protein concentration was determined using a bicinchoninic acid assay (Beyotime Biotechnology) and equalized before loading. Aliquots of 25–50 μg of protein were separated by SDS-PAGE and transferred onto polyvinylidene difluoride membranes (Millipore, MA, USA). Membranes were blocked and blotted with the relevant antibodies. Horseradish peroxidase-conjugated secondary antibodies were detected with an enhanced chemiluminescence reagent (Beyotime Biotechnology). Rho GTPase antibody sampler kit (CST, MA, USA) was used to determine the expression of the Ras homolog family member (Rho) of guanosine triphosphatases (GTPases). GAPDH was used as a loading control. All antibody dilutions were 1:1000 except for the GAPDH antibody, which was used at a dilution of 1:5000.

Cell proliferation assay

Cell suspension was inoculated in a 96-well plate ($3–5\times10^3$ cells in 100 μl/well) and then incubated in a humidified incubator (37 °C, 5 % CO_2). After 48 h, 10 μl of the CCK-8 solution (Dojindo Laboratories, Kumamoto, Japan) was added to each well, and then the plate was incubated for 2–4 h (37 °C, 5 % CO_2). Absorbance at 450 nm was measured using a microplate reader.

Cell migration assay

Cell migration assays were performed using a chamber (Corning, Tewksbury, MA, USA) with 8.0-μm polycarbonate filter inserts in 24-well plates. Briefly, the lower chamber was filled with 2 % (v/v) fetal bovine serum medium. HUVECs (5×10^4 cells/well) in a serum-free medium were added to the upper chamber. The cells were allowed to migrate for 12 h at 37 °C. The non-migrated cells were removed from the upper surface of the membrane by scraping with a cotton swab, and the migrated cells were fixed with methanol, stained with crystal violet, and photographed under an inverted microscope. Migration was assessed by counting the number of stained cells from 10 random fields at ×100 magnification.

Tube formation assay

The 96-well microplates (Corning, Tewksbury, MA, USA) were coated with Matrigel (65 μl/well) (Becton Dickinson, Piscataway, NJ, USA) and allowed to polymerize for 30 min at 37 °C. HUVECs were added at 2×10^4 cells/well into each well covered with Matrigel in 100 μl of a mixture of Matrigel and EGM-2 (2:1, v/v). Tube formation was recorded at different time points with an inverted microscope (Olympus, Tokyo, Japan) from five random fields at ×100 magnification.

Animal study

Male BALB/c nude mice (5 weeks old) were obtained from the Shanghai Institute of Materia Medica, Chinese Academy of Science, and housed under specific pathogen-free conditions. The experimental protocol was approved by the Shanghai Medical Experimental Animal Care Commission. Twenty-four mice were randomized into four groups: (1) HepG2 cells (5×10^6 cells) mixed with HUVEC-control cells (5×10^6 cells), (2) HepG2 cells (5×10^6 cells) mixed with HUVEC-kd-Robo1 cells (5×10^6 cells), (3) HCC-LM3 cells (5×10^6 cells) mixed with HUVEC-control cells (5×10^6 cells), or (4) HCC-LM3 cells (5×10^6 cells) mixed with HUVEC-oe-Robo1 cells (5×10^6 cells) in 200 μl normal Matrigel which were implanted by subcutaneous injection to obtain subcutaneous tumors. The tumor volumes were measured using a Vernier caliper every 4 days, and the mice were euthanized after 4 weeks. The tumor volume was calculated according to the following formula: tumor volume=(largest diameter× perpendicular height^2)/2.

Statistical analysis

Statistical analysis was performed with SPSS for Windows (version 13.0; SPSS Inc., Chicago, IL, USA). The association between expression of Robo1 on endothelial cells and clinicopathological variables was analyzed using Pearson's chi-square test or Fisher's exact test, as appropriate. Quantitative variables were analyzed using the independent samples t test. Time to recurrence were assessed using the Kaplan-Meier method and compared with the log-rank test. A P value <0.05 was considered statistically significant. Western blot, HUVEC tube formation, and IOD of filamentous actin (F-actin) was analyzed by ImageJ (National Institutes of Health, Bethesda, MD, USA).

Results

Robo1 can be detected on endothelial cells and tumor cells in HCC

CD31 staining was mainly found on the endothelial cells, whereas Robo1 expression was found on tumor cells (Fig. 1a, Supplementary Fig. S1a–c) and endothelial cells with a co-staining of CD31 (Fig. 1b). Tumor size was significantly associated with Robo1 expression on endothelial cells in tumor vessels ($P=0.025$; Supplementary Table 2). Furthermore, HUVECs and TECs isolated from tumor by CD31 antibody-conjugated magnetic beads from three patients were Robo1 positive (Fig. 1c–f), which was further validated by Western blot (Fig. 1g).
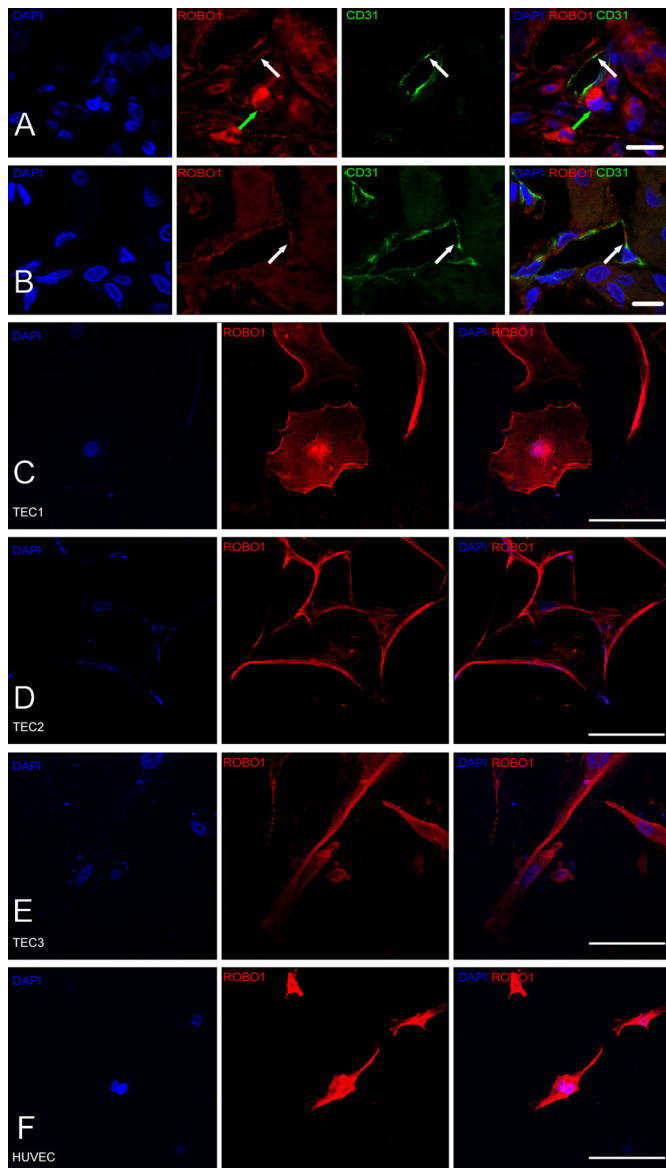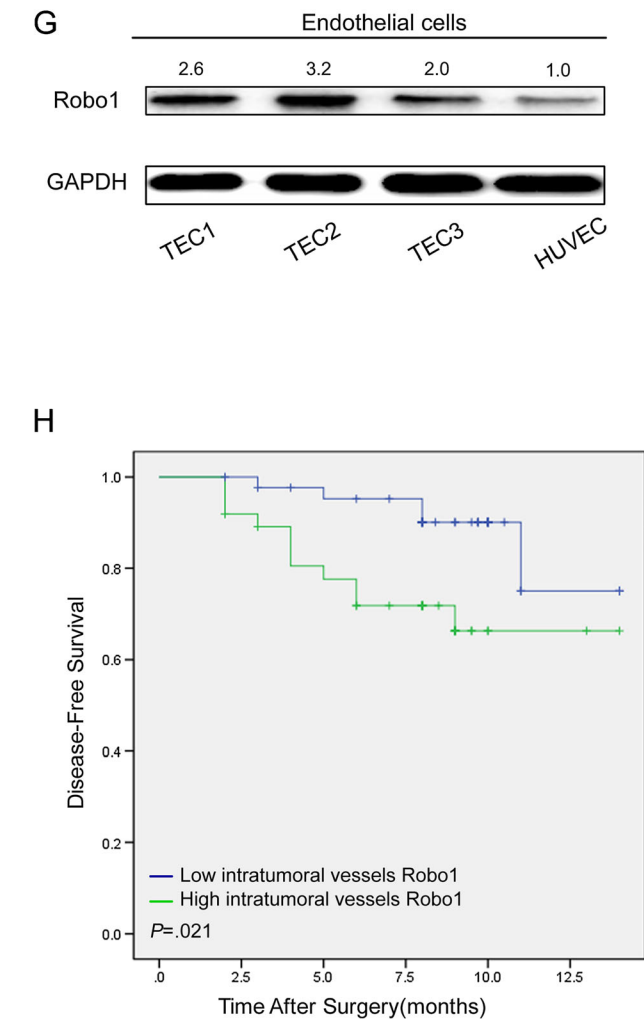

Fig. 1 Robo1 was found with co-staining of CD31 on endothelial cells in HCC, isolated tumor endothelial cells, and human umbilical vein endothelial cells. **a** Confocal laser scanning microscopy images of Robo1 expression on tumor cells and endothelial cells. CD31 (*green*) expression on endothelial cells. Robo1 and CD31 showed co-staining on tumor cells (*green arrows*) and endothelial cells (*white arrows*) in HCC. *Scale bars*=10.0 μm. **b** Confocal laser scanning microscopy images of Robo1 expression on angiogenesis endothelial cells. CD31 (*green*) expression on endothelial cells. Robo1 and CD31 showed co-staining on intratumoral endothelial cells (*white arrows*) in HCC. *Scale bars*=10.0 μm. **c–f** Confocal laser scanning microscopy images of Robo1 expression in isolated TECs and HUVECs. TECs [TEC1 (**c**), TEC2 (**d**), TEC3 (**e**)] isolated from three patients by CD31 antibody-conjugated magnetic beads were Robo1 positive and were found in HUVECs (**f**). DAPI was used to stain the cell nuclei (*blue*). *Scale bars*=100.0 μm. **g** Western blot validated Robo1 expression of TEC1, TEC2, TEC3, and HUVECs. GAPDH was used as the loading control. **h** High Robo1 expression on tumor vessels was associated with shorter disease-free survival ($P=0.021$)
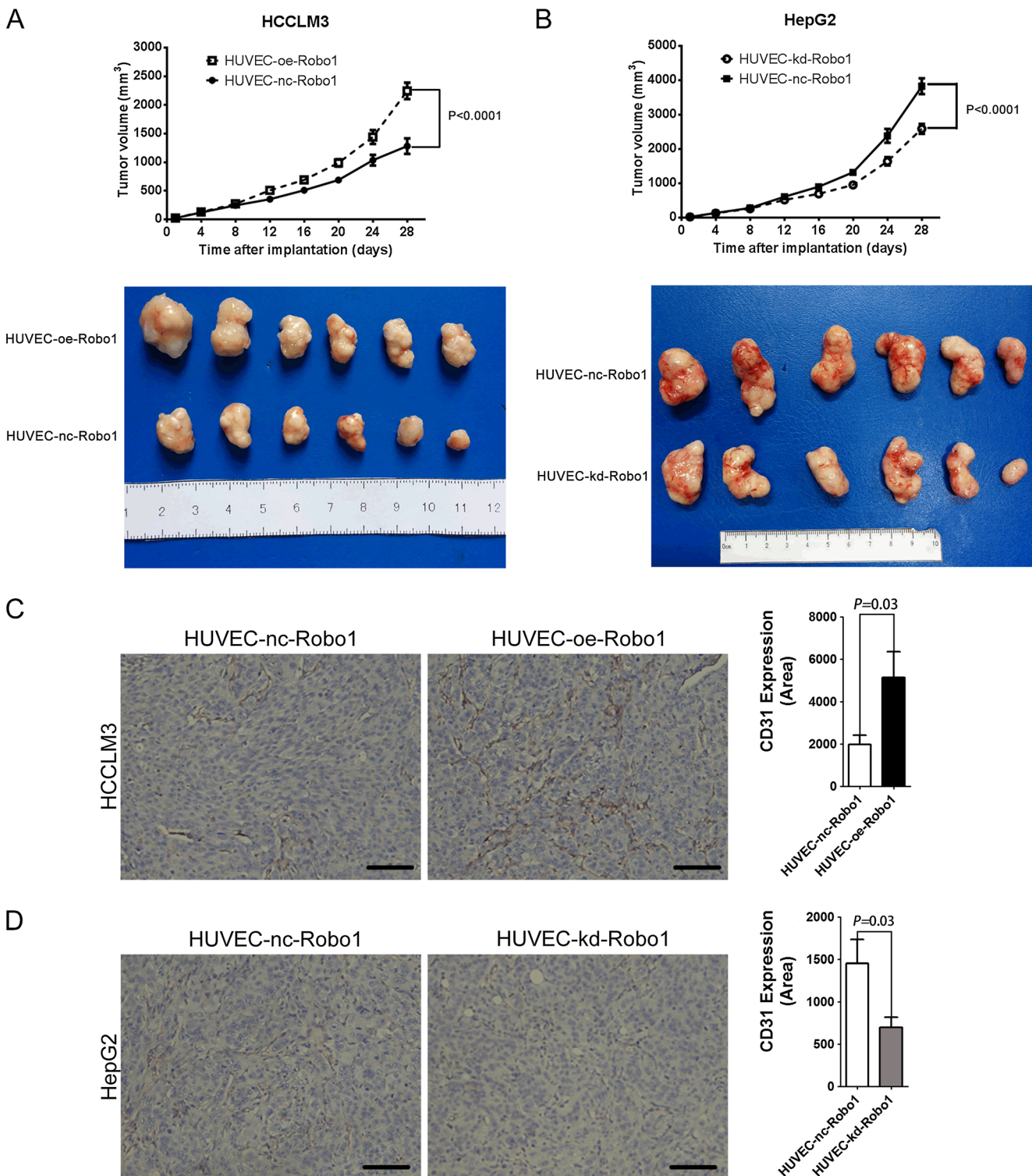
Fig. 2 HUVEC-kd-Robo1 decreased growth of HepG2 tumor size and HUVEC-oe-Robo1 accelerated HCCLM3 tumor volume by affecting tumor angiogenesis. Subcutaneous tumors derived from a xenograft model implanted with HepG2 or HCCLM3 mixed with HUVECs. **a** In comparison with HCCLM3 mixed with HUVEC-nc-Robo1 cells, HCCLM3 mixed with HUVEC-oe-Robo1 cells resulted in an increased volume ($P<0.0001$) of subcutaneous tumors in BALB/c nude mice. **b** HepG2 mixed with HUVEC-kd-Robo1 cells resulted in a decreased tumor volume in comparison with HepG2 mixed with HUVEC-nc-Robo1 cells ($P<0.0001$). **c** HCCLM3 cells mixed with HUVEC-oe-Robo1 cells had higher microvessel density than the control tumors ($P=0.030$). **c** HepG2 cells mixed with HUVEC-kd-Robo1 cells had lower microvessel density compared with the HepG2 cells mixed with HUVEC-nc-Robo1 ($P=0.030$)

High expression of Robo1 on endothelial cells is associated with poor prognosis

Robo1 expression on tumor cells was not associated with disease-free survival in cohort 1 (Supplementary Fig. S1c). Then, we focused on the implications of Robo1 expression on TECs. As shown in Supplementary Tables 1 and 2, the prognostic value of each clinicopathological feature was examined by univariate and multivariate analyses. In cohort 2, we divided the patients into subgroups with a high or low Robo1 expression on TECs. Robo1 expression on tumor vessels was significantly associated with diseases-free survival ($P=0.021$) (Fig. 1h).

Higher expression of Robo1 on HUVECs promoted tumor growth in xenograft model

To evaluate the role of Robo1 expression on endothelial cells in tumor growth, we examined its effects in a xenograft model implanted with HepG2 or HCCLM3 mixed with HUVECs. We found that tumor growth of HCCLM3 was increased when mixed with HUVEC-oe-Robo1 cells compared with HCCLM3 mixed with HUVEC-control-Robo1 ($P<0.0001$), whereas tumor growth of HepG2 was decreased when mixed with HUVEC-kd-Robo1 cells compared with HepG2 mixed with HUVEC-control cells ($P<0.0001$) (Fig. 2a, b).

We further examined microvessel density in the tumor samples. The HCCLM3 tumor cells mixed with HUVEC-oe-Robo1 cells had higher microvessel density than those mixed with HUVEC-nc-Robo1 cells ($P=0.030$; Fig. 2c). HepG2 tumor cells mixed with HUVEC-kd-Robo1 cells had lower microvessel density compared with those mixed with HUVEC-nc-Robo1 cells ($P=0.030$; Fig. 2d).

To further explore whether HUVECs participate in producing tumor vessels in the xenograft model, we examined tumor tissues containing mCherry-labeled Robo1-overexpressing HUVECs only and mCherry-labeled Robo1-knockdown HUVECs only by confocal laser scanning microscopy. Our observations indicated that mCherry-labeled HUVECs participate in functional tumor vessels containing erythrocytes in Robo1-overexpressing HUVECs (Fig. 3a), but not Robo1-knockdown HUVECs (Fig. 3b).

Higher expression of Robo1 promoted proliferation, tube formation, and migration of HUVECs by Rho GTPase pathway

We found HUVEC-kd-Robo1 cells changed to be spindle shaped (Fig. 4a–c) and had a decreased ability of tube formation, migration, and proliferation, whereas HUVEC-oe-Robo1 cells showed increased tube formation ,migration, and proliferation, as compared with controls (Fig. 4d–h).

Because Robo1 is involved in cell proliferation, cytoskeletal organization, and angiogenesis [11], we examined the expression of TGF-β, cyclin-D1, cyclin-dependent kinase 2 (CDK2), PCNA, EGFR, and Cdc42 by reverse transcription PCR. Of them, Cdc42 expression was significantly decreased in HUVEC-kd-Robo1 and increased in HUVEC-oe-Robo1 cells compared with the controls (Fig. 5a, b).

It has been reported that Robo1 affects the expression of several small GTPases [11, 24, 25], and we measured the expression of Cdc42, RhoA, RhoB, RhoC, and RAC1/2/3 in these cells by Western blot assay. The results showed that expression levels of Cdc42, RhoA, RhoB, and RhoC, but not RAC1/2/3, were increased in HUVEC-oe-Robo1 cells and decreased in HUVEC-kd-Robo1 cells (Fig. 5c).
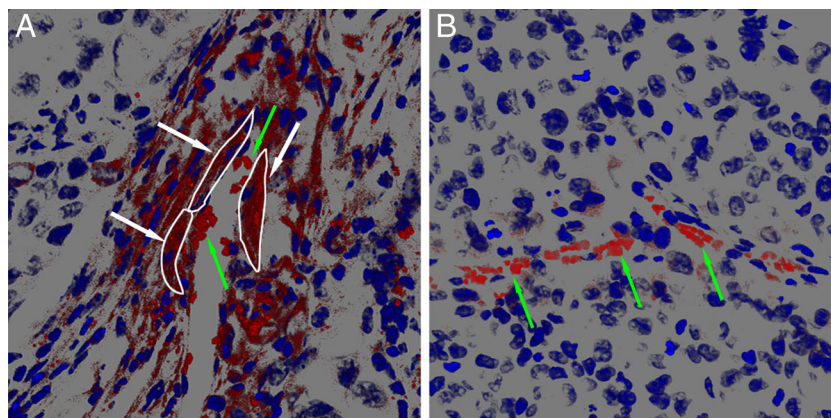

Fig. 3 Robo1-overexpressing HUVECs participate in producing tumor vessels. Images of tumor tissues were observed by confocal laser scanning microscopy. HCCLM3 tumors mixed with mCherry-labeled Robo1-overexpressing HUVECs and HepG2 tumors mixed with mCherry-labeled Robo1-knockdown HUVECs were examined. **a** Blood vessels in subcutaneous tumors of HCCLM3 tumors mixed with mCherry-labeled Robo1-overexpressing HUVECs were partly composed of mCherry-labeled Robo1-overexpressing HUVECs (shown by *white arrow* and *white outlines*; erythrocytes are anucleate cells pointed by *green arrows*) in a reconstructed image. **b** Blood vessels in subcutaneous tumors of HepG2 tumors mixed with mCherry-labeled Robo1-knockdown HUVECs were found to have very few mCherry-HUVECs cell participating in functional tumor vessels (anucleate erythrocytes were shown as *green arrows*)
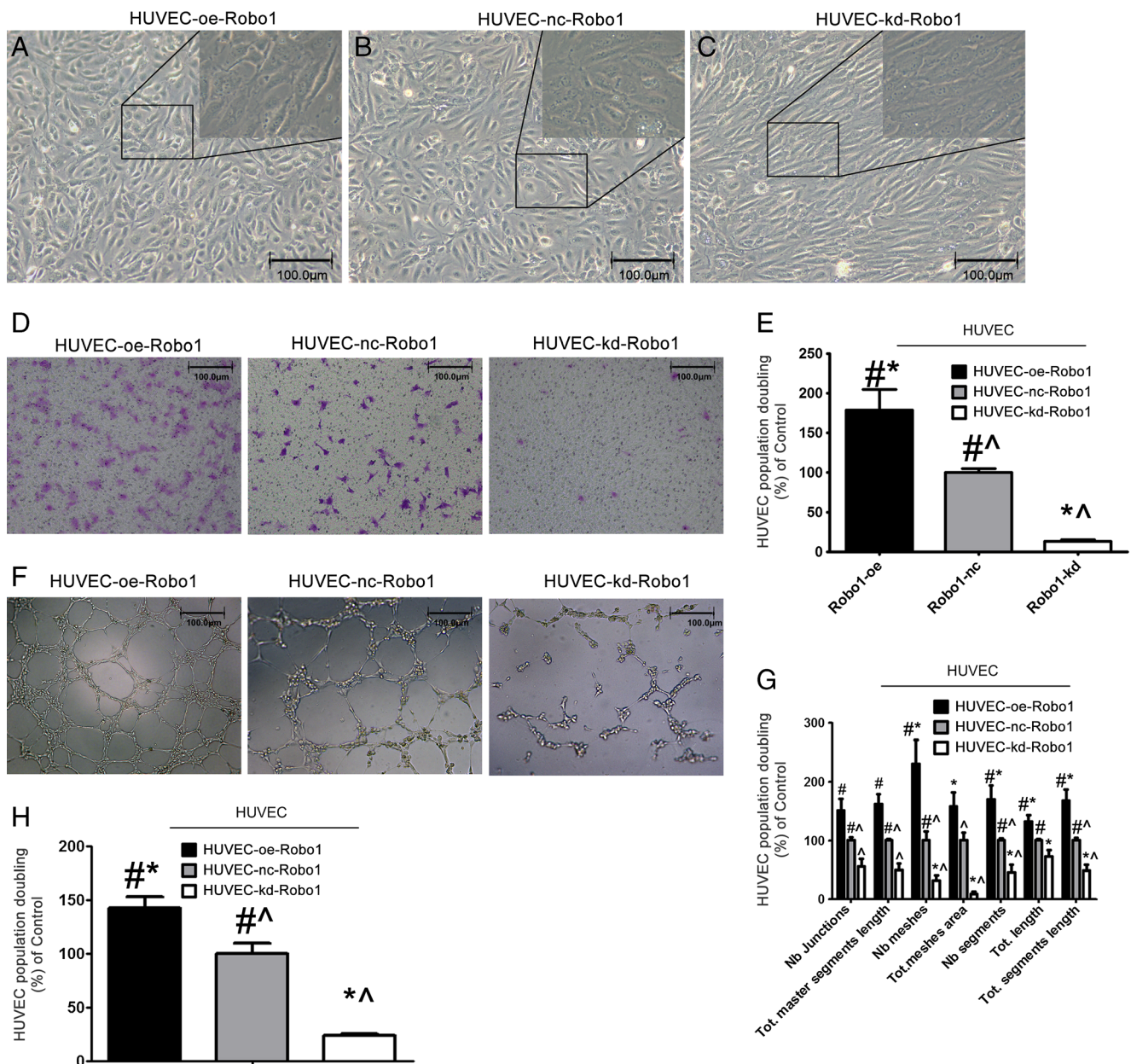
Fig. 4 Robo1-overexpressing HUVECs result in enhanced motility, tube formation, and proliferation, while Robo1-knockdown HUVECs are just the opposite. Representative photographs of HUVEC-oe-Robo1 (**a**), HUVEC-nc-Robo1 (**b**), and HUVEC-kd-Robo1 (**c**). HUVEC migration (**d**, **e**), tube formation (**f**, **g**), and proliferation (**h**) were assessed in HUVEC-oe-Robo1, HUVEC-nc-Robo1, and HUVEC-kd-Robo1 cells. The tube length and the number of migrating cells were evaluated by counting 10 random fields at ×100 magnification. ($^P<0.05$ compared with HUVEC-oe-Robo1; $^*P<0.05$ compared with HUVEC-nc-Robo1; $^#P<0.05$ compared with HUVEC-kd-Robo1)

Robo1 affected filamentous actin organization in HUVECs

Because Cdc42 and RhoA GTPases are known to modulate actin cytoskeleton organization in cells [26–28], we examined F-actin organization in HUVEC-oe-Robo1, HUVEC-nc-Robo1, and HUVEC-kd-Robo1 cells. We found distortion of F-actin in HUVEC-kd-Robo1 cells, and the F-actin expression was highest in HUVEC-oe-Robo1 (Supplementary Fig. S2).

Blocking Cdc42 eliminated the differences in F-actin distortion, migration, and tube formation among HUVEC-oe-Robo1, HUVEC-nc-Robo1, and HUVEC-kd-Robo1

To explore whether the effect of Robo1 expression on cytoskeleton organization is mediated via Cdc42, we knocked down Cdc42 expression in HUVEC-oe-Robo1 cells, HUVEC-kd-Robo1 cells, and HUVEC-nc-Robo1 cells by the siRNA approach. Knockdown of Cdc42 attenuated the

Fig. 5 Robo1-overexpressing HUVECs result in increased Cdc42, RhoA, RhoB, and RhoC expression, while Robo1-knockdown HUVECs result in decreased Cdc42, RhoA, RhoB, and RhoC expression. Cell proliferation and cytoskeleton- or angiogenesis-relative mRNA levels and small GTPase expression were evaluated in HUVEC-oe-Robo1, HUVEC-nc-Robo1, and HUVEC-kd-Robo1 cells. **a**, **b** Cell proliferation and cytoskeleton- or angiogenesis-relative mRNA change after HUVECs were transfected by vectors. **c** The expression levels of Robo1, Cdc42, RhoA, RhoB, RhoC, and RAC in HUVEC-oe-Robo1, HUVEC-nc-Robo1, and HUVEC-kd-Robo1 cells were assessed. GAPDH was used as a loading control
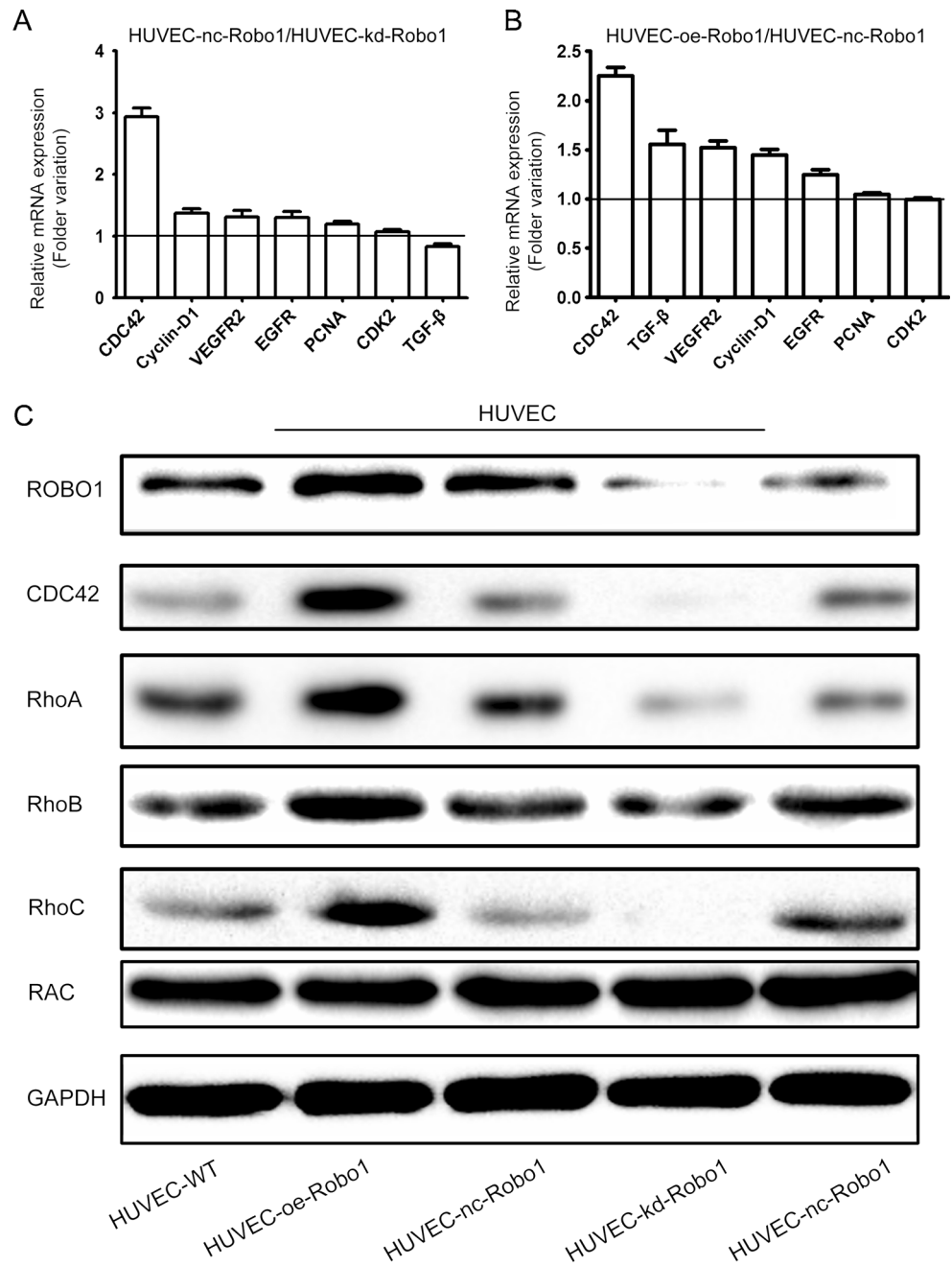
differences in F-actin organization (Fig. 6a, b), migration (Fig. 6c, d), and tube formation (Fig. 6e, f) among HUVEC-oe-Robo1, HUVEC-nc-Robo1, and HUVEC-kd-Robo1.

Discussion

Although several treatments targeting VEGF and VEGFR have been introduced into clinical practice, its modest effect and presence of tumor rebound encourage us to explore other regulators in tumor angiogenesis. Previous studies showed that the Slit-Robo1 interaction plays an important role in angiogenesis, the interruption of this interaction resulted in a decrease in tumor growth and angiogenesis [11, 29], and the direct inhibition of Robo1 expression in endothelia cells by the siRNA approach also inhibited cell migration and tube formation [30]. However, how Robo1 affects endothelial cells and the role of Robo1 in HCC remains to be clarified.

The present study showed knockdown of Robo1 expression in HUVECs resulted in decreased proliferation, migration ability, and tube formation. The present study also revealed that the pro-angiogenesis effect of Robo1 expression in endothelial cells is mediated by modulation of Rho family of GTPases and cytoskeleton. The Rho family of GTPases,
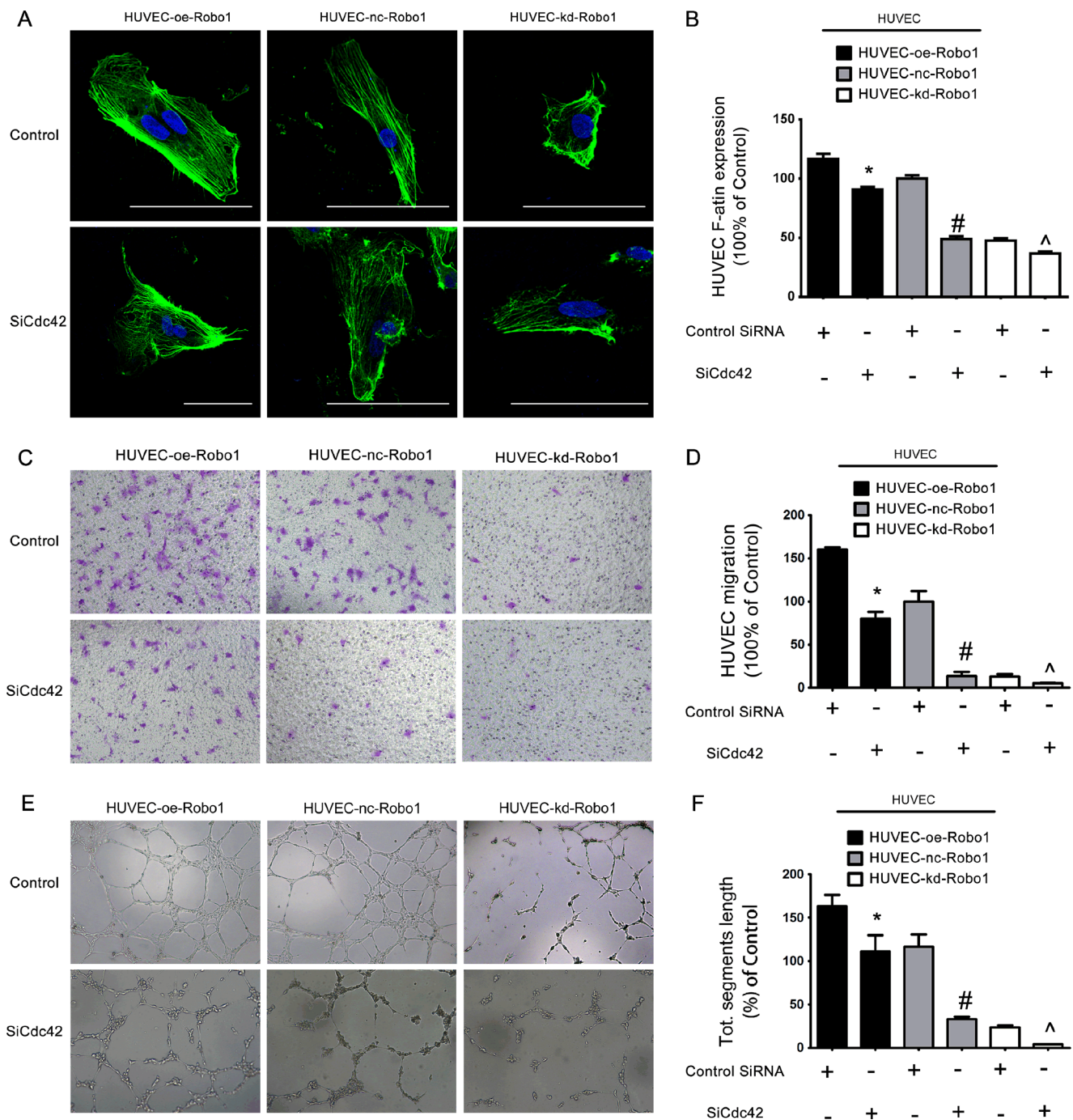
Fig. 6 Cdc42 siRNA treatment eliminated differences in F-actin distortion, migration, and tube formation between HUVEC-oe-Robo1, HUVEC-nc-Robo1, and HUVEC-kd-ROBO1 cells. Comparisons of the effects of Cdc42 siRNA treatment of F-actin expression (a, b), migration (c, d), and total segment lengths of tube formation (e, f) among HUVEC-oe-Robo1, HUVEC-nc-Robo1, and HUVEC-kd-Robo1 cells. (^$P<0.05$, Cdc42 siRNA-treated HUVEC-oe-Robo1 compared with HUVEC-oe-Robo1; *$P<0.05$, Cdc42 siRNA-treated HUVEC-nc-Robo1 compared with HUVEC-nc-Robo1; #$P<0.05$, Cdc42 siRNA-treated HUVEC-kd-Robo1 compared with HUVEC-kd-Robo1; while $P>0.05$, Cdc42 siRNA-treated HUVEC-oe-Robo1 compared with HUVEC-nc-Robo1; $P>0.05$, Cdc42 siRNA-treated HUVEC-nc-Robo1 compared with HUVEC-kd-Robo1)

including Rho, Rac, and Cdc42, has been implicated in many cellular processes, including actin and microtubule cytoskeleton organization, and they also can influence cell polarity, microtubule dynamics, membrane transport pathways, and transcription factor activity [31–33]. Furthermore, it was recently reported that active Cdc42 promoted the extension of endothelial filopodia to facilitate angiogenic sprouting [34]. The present study is also in line with the report showing that

the inhibition of RhoC/Rac GTPase activation resulted in a decreased angiogenesis in HCC [35]. It was reported that Robo1 regulated the Rho family of GTPase families in neuronal cells [36]. To our knowledge, this is the first study to show how Robo1 affects endothelial cells, and support that neuronal cells and endothelial cells share the same pathway in regulating cell migration and structure; however, the regulatory mechanism of Robo1 expression in tumor endothelial cells is still unclear.

The role of Robo1 expression on tumor cells remains controversial. In colorectal cancer, Robo1 plays a role of oncogene, while in cervical, kidney, breast, and lung cancer, Robo1 is a tumor suppressor gene [37]. We noticed that several previous studies showed that Robo1 was overexpressed in HCC tumor tissues quantitated by real-time PCR and associated with a higher AFP level, tumor stage, and poorer differentiation [38]; however, the present study did not support the relation between the expression of Robo1 on tumor cells and the patients' survival; therefore, we did not explore the role of Robo1 expression on tumor cells in HCC.

The present study showed that Robo1 expression promoted tumor angiogenesis and tumor growth in HCC, and its expression on tumor endothelial cells associated with patients' survival, which supported that Robo1 could be a prognostic marker for HCC; more importantly, it may provide an alternative target for anti-angiogenesis treatment.

Conflicts of interest None

Authors' contributions JYA, ZTC, YYZ, and LQK performed the experimental work. NZ, BGY, HC, and DMG participated in the experiments. HCS participated in its design and coordination. The manuscript was written by HCS, JYA, and CTZ.

References

1. Jemal A, Bray F, Center MM, Ferlay J, Ward E, Forman D. Global cancer statistics. CA. 2011;61:69–90.
2. Poon RT, Ng IO, Lau C, Zhu LX, Yu WC, Lo CM, et al. Serum vascular endothelial growth factor predicts venous invasion in hepatocellular carcinoma: a prospective study. Ann Surg. 2001;233: 227–35.
3. Sugimachi K, Tanaka S, Terashi T, Taguchi K, Rikimaru T, Sugimachi K. The mechanisms of angiogenesis in hepatocellular carcinoma: angiogenic switch during tumor progression. Surgery. 2002;131:S135–41.
4. Tanigawa N, Lu C, Mitsui T, Miura S. Quantitation of sinusoid-like vessels in hepatocellular carcinoma: its clinical and prognostic significance. Hepatology. 1997;26:1216–23.
5. Llovet JM, Hernandez-Gea V. Hepatocellular carcinoma: reasons for phase III failure and novel perspectives on trial design. Clin Cancer Res. 2014;20:2072–9.
6. Carmeliet P. Blood vessels and nerves: common signals, pathways and diseases. Nat Rev Genet. 2003;4:710–20.
7. Eichmann A, Le Noble F, Autiero M, Carmeliet P. Guidance of vascular and neural network formation. Curr Opin Neurobiol. 2005;15:108–15.
8. Alpar A, Tortoriello G, Calvigioni D, Niphakis MJ, Milenkovic I, Bakker J, et al. Endocannabinoids modulate cortical development by configuring Slit2/Robo1 signalling. Nat Commun. 2014;5:4421.
9. Borrell V, Cardenas A, Ciceri G, Galceran J, Flames N, Pla R, et al. Slit/Robo signaling modulates the proliferation of central nervous system progenitors. Neuron. 2012;76:338–52.
10. Mehlen P, Delloye-Bourgeois C, Chedotal A. Novel roles for slits and netrins: axon guidance cues as anticancer targets? Nat Rev Cancer. 2011;11:188–97.
11. Wang B, Xiao Y, Ding BB, Zhang N, Yuan X, Gui L, et al. Induction of tumor angiogenesis by Slit-Robo signaling and inhibition of cancer growth by blocking Robo activity. Cancer Cell. 2003;4:19–29.
12. Chang PH, Hwang-Verslues WW, Chang YC, Chen CC, Hsiao M, Jeng YM, et al. Activation of Robo1 signaling of breast cancer cells by Slit2 from stromal fibroblast restrains tumorigenesis via blocking PI3k/Akt/beta-catenin pathway. Cancer Res. 2012;72: 4652–61.
13. Parray A, Siddique HR, Kuriger JK, Mishra SK, Rhim JS, Nelson HH, et al. Robo1, a tumor suppressor and critical molecular barrier for localized tumor cells to acquire invasive phenotype: study in African-American and Caucasian prostate cancer models. Int J Cancer (Journal International du Cancer). 2014;135:2493–506.
14. Je EM, Gwak M, Oh H, Choi MR, Choi YJ, Lee SH, et al. Frameshift mutations of axon guidance genes Robo1 and Robo2 in gastric and colorectal cancers with microsatellite instability. Pathology. 2013;45:645–50.
15. Qi C, Lan H, Ye J, Li W, Wei P, Yang Y, et al. Slit2 promotes tumor growth and invasion in chemically induced skin carcinogenesis. Lab Investig. 2014;94:766–76.
16. Alajez NM, Lenarduzzi M, Ito E, Hui AB, Shi W, Bruce J, et al. MiR-218 suppresses nasopharyngeal cancer progression through downregulation of survivin and the SLIT2-ROBO1 pathway. Cancer Res. 2011;71:2381–91.
17. Shao Y, Zhou Y, Hou Y, He J, Hu L, Zhang Y, et al. Prognostic implications of SLIT and ROBO1 expression in gallbladder cancer. Cell Biochem Biophys. 2014;70:747–58.
18. Ito H, Funahashi S, Yamauchi N, Shibahara J, Midorikawa Y, Kawai S, et al. Identification of ROBO1 as a novel hepatocellular carcinoma antigen and a potential therapeutic and diagnostic target. Clin Cancer Res. 2006;12:3257–64.
19. Roayaie S, Blume IN, Thung SN, Guido M, Fiel MI, Hiotis S, et al. A system of classifying microvascular invasion to predict outcome after resection in patients with hepatocellular carcinoma. Gastroenterology. 2009;137:850–5.
20. Zhu XD, Zhang JB, Zhuang PY, Zhu HG, Zhang W, Xiong YQ, et al. High expression of macrophage colony-stimulating factor in peritumoral liver tissue is associated with poor survival after curative resection of hepatocellular carcinoma. J Clin Oncol. 2008;26: 2707–16.
21. Xiong YQ, Sun HC, Zhang W, Zhu XD, Zhuang PY, Zhang JB, et al. Human hepatocellular carcinoma tumor-derived endothelial cells manifest increased angiogenesis capability and drug resistance compared with normal endothelial cells. Clin Cancer Res. 2009;15: 4838–46.

22. Kong J, Kong J, Pan B, Ke S, Dong S, Li X, et al. Insufficient radiofrequency ablation promotes angiogenesis of residual hepatocellular carcinoma via HIF-1alpha/VEGFA. PLoS One. 2012;7:e37266.

23. Strohmaier AR, Porwol T, Acker H, Spiess E. Tomography of cells by confocal laser scanning microscopy and computer-assisted three-dimensional image reconstruction: localization of cathepsin B in tumor cells penetrating collagen gels in vitro. J Histochem Cytochem. 1997;45:975–83.

24. Yang YH, Manning Fox JE, Zhang KL, MacDonald PE, Johnson JD. Intraislet SLIT-ROBO signaling is required for beta-cell survival and potentiates insulin secretion. Proc Natl Acad Sci U S A. 2013;110:16480–5.

25. Geutskens SB, Hordijk PL, van Hennik PB. The chemorepellent Slit3 promotes monocyte migration. J Immunol. 2010;185:7691–8.

26. Valtcheva N, Primorac A, Jurisic G, Hollmen M, Detmar M. The orphan adhesion G protein-coupled receptor GPR97 regulates migration of lymphatic endothelial cells via the small GTPases RhoA and CDC42. J Biol Chem. 2013;288:35736–48.

27. Ni S, Hu J, Duan Y, Shi S, Li R, Wu H, et al. Down expression of LRP1B promotes cell migration via RhoA/Cdc42 pathway and actin cytoskeleton remodeling in renal cell cancer. Cancer Sci. 2013;104:817–25.

28. Hall A. Rho GTPases and the actin cytoskeleton. Science. 1998;279:509–14.

29. Wang LJ, Zhao Y, Han B, Ma YG, Zhang J, Yang DM, et al. Targeting slit-roundabout signaling inhibits tumor angiogenesis in chemical-induced squamous cell carcinogenesis. Cancer Sci. 2008;99:510–7.

30. Huang L, Xu Y, Yu W, Li X, Liqun C, He X, et al. Robo1: a potential role in ocular angiogenesis. Curr Eye Res. 2009;34:1019–29.

31. Jaffe AB, Hall A. Rho GTPases: biochemistry and biology. Annu Rev Cell Dev Biol. 2005;21:247–69.

32. Raftopoulou M, Hall A. Cell migration: Rho GTPases lead the way. Dev Biol. 2004;265:23–32.

33. Etienne-Manneville S, Hall A. Rho GTPases in cell biology. Nature. 2002;420:629–35.

34. Wakayama Y, Fukuhara S, Ando K, Matsuda M, Mochizuki N. Cdc42 mediates Bmp-induced sprouting angiogenesis through Fmnl3-driven assembly of endothelial filopodia in zebrafish. Dev Cell. 2015;32:109–22.

35. Zheng F, Liao YJ, Cai MY, Liu TH, Chen SP, Wu PH, et al. Systemic delivery of microRNA-101 potently inhibits hepatocellular carcinoma in vivo by repressing multiple targets. PLoS Genet. 2015;11:e1004873.

36. Wong K, Ren XR, Huang YZ, Xie Y, Liu G, Saito H, et al. Signal transduction in neuronal migration: roles of GTPase activating proteins and the small GTPase Cdc42 in the Slit-Robo pathway. Cell. 2001;107:209–21.

37. Legg JA, Herbert JM, Clissold P, Bicknell R. Slits and roundabouts in cancer, tumour angiogenesis and endothelial cell migration. Angiogenesis. 2008;11:13–21.

38. Avci ME, Konu O, Yagci T. Quantification of SLIT-ROBO transcripts in hepatocellular carcinoma reveals two groups of genes with coordinate expression. BMC Cancer. 2008;8:392.